Volume 15, Issue 2, 152416 (1-6)

International Journal of Industrial Chemistry (IJIC)

https://dx.doi.org/10.57647/j.ijic.2024.1502.16

Synthesis of photocatalytic material based on polyaniline supported PVC/$NiAl_2O_3$/AlF_3 nanocomposite

Ilnaz Ahmadian[1], Maryam Kargar Razi[1]*, Babak Sadeghi[2], Mahbobeh Nakhaei[1]

[1]*Department of Chemistry, Islamic Azad University, North Tehran Branch, Tehran, Iran.*
[2]*Department of Chemistry, Islamic Azad University, Tonekabon Branch, Tonekabon, Iran.*

*__Corresponding author:__ mkargarrazi@yahoo.com

Original Research

Received:
26 May 2024
Revised:
1 July 2024
Accepted:
4 July 2024
Published online:
30 July 2024

Abstract:

In this research, photocatalysis single AlF3, Ternary PVC/Al2O3/AlF3 (PNA) and polyaniline (PAI) supported PNA nanocomposite were synthesized by co-precipitation method. Surface area and morphological structure of the synthesized photocatalysts were characterized by X-ray Diffractometer (XRD), Brunauer-Emmett-Teller (BET), and Scanning Electron Microscopy (SEM). With the best conditions, the response in the glassy carbon electrode (GCE) showed concentrations of the malathion in the range values of 1.5-11 $\times 10^{-7}$ M, high recovery values around 98.4% with the good reproducibility. The stunning simplicity for preparation, and selectivity of this nanostructure and high sensitivity of polyaniline supported PNA electrode can make it a good candidate for application in detection of malathion.

Keywords: SEM; Photocatalytic effect; GCE, Malathion; Nanocomposite

1. Introduction

Light translucency and high specificity are some of the properties of aluminum fluoride nanoparticles that have been used and shown a wide range of applications [1, 2]. Hence, there have been numerous studies on nano-metal oxides and their number is continuing to increase. The compounds (MO = Metal oxides) are widely used and have numerous applications, including nanocatalysts, provide assistance for sensors, industrial catalysts, etc. [1–6]. Pure and inorganic hybrid materials can be produced using nano-metal oxides, which have been extensively developed through synthesis using the sol-gel method [7, 8]. Aluminium derivatives (Al_2O_3, $nAlF_3$, etc.) can also be used as catalyst support, which is another common application. Sol-gel processes are influenced by the performance of the catalyst due to the temperature, pH, raw materials, preparation technique, and time [9–11]. Ono *et al.* [12] was to report the effectiveness of the pH on the some oxides of Al formation. Meanwhile, used pH-swing and other techniques to prepare the catalyst supported by alumina [13]. The melting point can be lowered by aluminum fluoride in several current and potential applications and Enhance the electrical conductivity of the additive used in the aluminum production cell's molten electrolyte. In between MF_n (metal fluoride) catalysts and catalyst supports, AlF_3 is considered to be one of the most significant catalysts [14–18]. Sol-gel, sputtering, and chemical vapor depositing are among the methods used to prepare $nAlF_3$ (nAF) thin films. The sol-gel method is the most frequently employed method. Sol-gel methods were used to synthesize a thin film of nAF on a glass plate in this research (Fig. 1). Coating some metals with the AS is an easy and neutral solution [13]. We have created a method that reduces Ag nanoparticles (nanospheres to nanorods) [19], nanoplates [20], their antibacterial activity [21, 22], an improved an easy synthetic poly (diallyldimethylammonium chloride) (PDDA) [23], synthesis of Gold/HPC nanocomposite [24], Ag/ZnO nanocomposite [25, 26], and comparison of particles and plate shapes for the oxidation of ascorbic acid [27].

CuO/ZnO, TiO_2, CeO_2, CeO_2/ZnO, ZnO, SnO_2/ZnO, and CeO_2/CdS, are some of the photocatalysts and

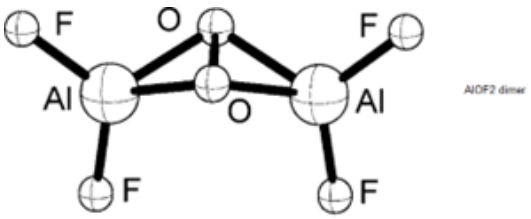

Figure 1. Schematic of $AlOF_2$ dimer sol (AS).

semiconductor nanoheterostructure materials developed so far [28–34]. The synthesis of metal-oxid compounds has long been considered the one of the perfect strategy for study and developing photocatalytic effect. Finally, this study to make a chemical photocatalyst using PNA and polyaniline as a carrier with heterostructure compounds.
It is our understanding that there are not many photocatalytic applications for polyaniline-based $PVC/NiAl_2O_3/AlF_3$ (PNA) nanocomposites. In this work, a new material as a target contaminant has been developed and analyzed to investigate its capability of detecting the pesticide malathion.

2. Experimental

2.1 Synthesis of photocatalysts

Changes in the crystalline structures provided in the XRD are highlighted for the chemical reactions (reaction 1) that occurred during the preparation. This sample had Nano Aluminum Fluoride (nAF) used as a precipitant, so it can be concluded [15, 16].

$$Al(CH_3COO)_3 + Al_2O_2F_4 + 5\,HF \xrightarrow[\text{In glass reactor}]{\text{Alkaline regions}} 3\,\text{nano}AlF_3 + 3\,CH_3COOH + H_2 + O_2 \quad (1)$$

$$(\text{NH3 solvent}) \longrightarrow (\text{nAF})$$

Taking the proper amounts of the initial single nAF powder was the basis for synthesizing the ternary nanocomposites and AlF_3 nanoparticle precursors have diverse molar ratios when added to deionize water. Typical procedures involve dissolved 0.1 mL of nAF powder in deionized water and sonicating it for 2 hours. The sonication process continued with the introduction of 0.1 M $Ni(CH_3COO)_2$ and an additional 2 hours of sonication. Over four hours, the solution was continuously stirred while dropwise adding $K_2S.9H_2O$ of the same molarity. A PNA nanocomposite was thought to be the result of the product [14].
The filtered precipitate was divided, water and ethanol. Then precipitate dried at 90 °C for 10 hours in an oven, after calcination at 180 °C for 1.5 hours. In the experimental synthesized nanoparticles, aniline has been polymerized using typical oxidative polymerization methods [15, 16]. The preparation of $PVC/NiAl_2O_3/AlF_3$ (PNA) nanocomposites on polyaniline (PAI) supports took place using 0.2 M of aniline and Hydrocholoroc acid dissolved and then for 15 min stirred. The aniline solution was mixed with 3 grams of PNA and stirred for 20 minutes before being stirred with ice water bath for 1.5 hours. After 3 hours, filtered water, deionized water, and ethanol were used to separate the precipitate, and then it was dry at 70 °C for 9 hours. Immediately, the solution turned white and then gray, and this precipitation was labeled as a PNA nanocomposition on polyaniline support [17, 27–34].
The structures of the photocatalyst have been characterized by XRD (at step scan rate of 0.03° (2θ = 7.0 to 92.2°, CuKα radiation (λ=0.16 nm) using 50 kV and 45 mA).
Solid morphologies and particle dispersion of the synthesized photocatalyst have been studied and evaluated (initial concentration 25 mg/L) the effect of pH= 4.0-10.0.
Malathion was added to the sample after washing the tomato samples water and divides them into some small portions. Then, at a known concentration and then examined using the proposed sensor.

3. Results and Discussion

3.1 Characterization of the synthesized photocatalysts - XRD analysis of the as-synthesized photocatalyst

As shown in Fig. 1, the XRD profiles of the synthesized $PVC/NiAl_2O_3/AlF_3$ (PNA) photocatalyst and the polyaniline-supported PNA were determined. As a result, the observed diffraction peaks at the observed at 2θ of 29.11, 32.29, 47.41, 56.19, 60.05, 70.09, 77.04, 80.09 and 88.54° for scattering angle and represent the cubic shape for Al fluorite [35, 36].
In the $NiAl_2O_3/AlF_3$, sharp observed diffraction peaks for the AlF_3 nanoparticle, are due to the cubic fluorite structure. In the other hand, at 2θ values of 26.62, 43.37 and 51.98° for the diffraction peaks, show hexagonal structure for the AlF_3 [35, 37, 38].
The pattern of the XRD for PVC/AlF_3 is very something similar to that of CdS pure salt, and do not change for PVC the diffraction peak positions, showing that AlF_3 is not integrated into the PVC lattice [26, 36].
This three-component system was observed for certain values of 2θ and provided different diffraction peaks. Among them, at 2θ values of 28.05, 33.76, 48.06 and 56.01° for the diffraction peaks can be appearance to the cubic fluorite structure of the AlF3 nanoparticle. The 2θ peaks of 29.62, 33.02, 33.28, 33.99, 36.99, 52.90 and 69.89° can be presentation to cubic PVC structure, while the 2θ peaks of 26.5, 33.5, 27.81, 28.72, 43.21 and 46.91° can be assigned to the body center hexagonal structure of CdS [26].
Several diffraction peaks that given 2θ in the support system, as shown in Fig. 2. For the reaction of $PVC/NiAl_2O_3/AlF_3$ (PNA) with polyaniline, some diffraction peaks for $NiAl_2O_3$, PVC and AlF_3 may go away. This confirms the effectiveness of the polyaniline coating on the

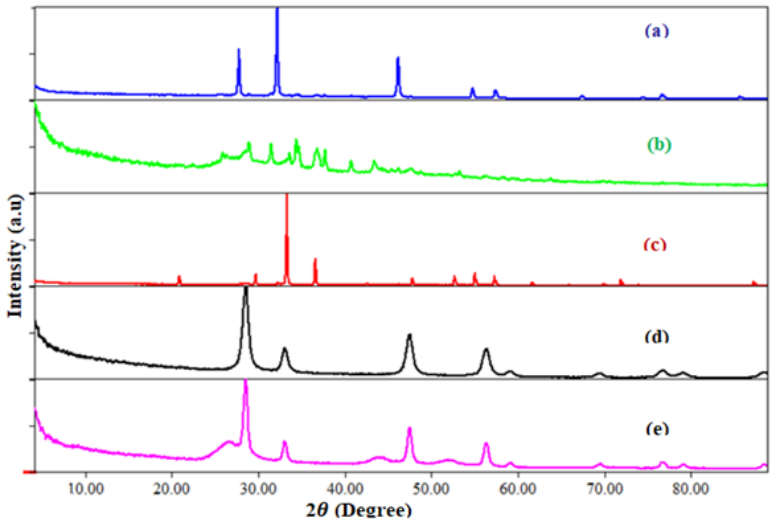

Figure 2. XRD spectra of a) PAI supported PVC/$NiAl_2O_3$/AlF_3, b) PVC/$NiAl_2O_3$/AlF_3 (4:1), c) PVC/ AlF_3, d) AlF_3, e) $NiAl_2O_3$/AlF_3.

PNA surface. The crystallite size of the synthesized photocatalysts was calculated and provided using the Debye-Scherrer formula [30];

$$D = \frac{K\lambda}{\beta \cos\theta} \tag{2}$$

where, D is crystallite size (nm), K = aspect ratio constant taken as 0.9; β is the full width at half maximum (FWHM) in radians, λ is the X-ray wavelength (0.16 nm) for the Kα1 radiation of the Cu target and θ is the Bragg angle. Overall, the calculated average crystal size of the synthesized photocatalyst confirms the contribution of a good nanocrystal range of 30–40 nm [30, 31], as summarized in Table 1.

- Surface area determining

For determined of the synthesized nanocomposites and improving the sensitivity of sensors the Brunauer-Emmett-Teller (BET) method is an important factor. For the each sample the specific surface area (SSA) is determining and examined by isothermal nitrogen adsorption-desorption analysis (Table 2). For AlF_3 (71.375 m^2g^{-1}) the specific surface area is highest, while it is lowest for PVC (0.520 m^2g^{-1}), providing its compact nature. The binary system of $NiAl_2O_3$/AlF_3 has a specific surface area near to the $NiAl_2O_3$ (69.9 m^2g^{-1}). A specific surface area (approx. 4.9 m^2g^{-1}) was calculated for PVC/AlF_3. The SSA can be arranging and showed in table 2 (39.9 and 19.4 m^2g^{-1}) for the supported nanocomposite.

- Study of the SEM image and TGA

The morphological of photocatalysts; PNA and polyaniline-supported PNA were tested, as shown in Figs. 3a–b. It can be seen for the nano AlF_3 are distributed in the surface of PVC and the $NiAl_2O_3$ particles in the form of the central shell. The SEM image without clear morphology of the nanocomposite provided and showed shape and size nanoparticles (Figs. 3a–b). Some metals including Ni and Al showed to the brighter particles in the polyaniline system.

The thermal behavior of dried nAlF_3 by TG-DTG analysis is highlighted in Fig. 4. As displayed, the variation between these two samples results from the presence of alumina precipitates. In Fig. 4, the TG curve reveals three-stage weight loss that can be used to explain the thermal transformation of pseudo-boehmite into nAlF_3. At temperatures less than 100 °C, about 7.63% a decrease in weight is associated with the evaporation of adsorbed water molecules that exist in pseudo-boehmite pores, which releases O_2, NH_3, H_2 and forms nAlF_3 nanoparticles. When the temperature increased from 310 to 500 °C, the weight loss of 2.5% is related to the removal of the remaining acetates in the crystalline structure of nAlF_3.

Table 1. Crystal size of as-synthesized photocatalysts.

As-synthesized photocatalyst	2θ (°)	β (radians)	D (nm)
PVC/$NiAl_2O_3$/AlF_3 (4 : 1)	34.40	0.00414	36.0
PANI- PVC/$NiAl_2O_3$/AlF_3	32.19	0.00442	31.7

Table 2. SSA of the synthesized photocatalysts.

photocatalyst	Surface area with BET (m^2g^{-1})
PVC/$NiAl_2O_3$/AlF_3	39.9±0.041
PANI- PVC/$NiAl_2O_3$/AlF_3	19.4±0.082

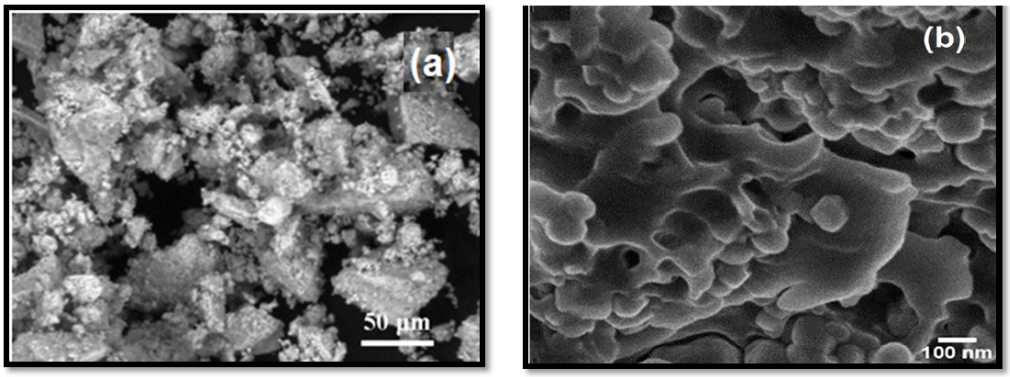

Figure 3. The SEM images: (a) PVC/$NiAl_2O_3$/AlF_3, (b) polyaniline supported PVC/$NiAl_2O_3$/AlF_3 photocatalyst.

3.2 Electrode pH optimization with polyaniline supported PVC/$NiAl_2O_3$/AlF_3

The effect of the pH on the sensor response in a solution of 4×10-7 M malathion in 0.2 M KCl was studied. The changing of the pH in the solution help to affects the characteristic of the sensors. The connection among the pH of the solution and its interaction to malathion detection is provided in Fig. 5. The pH value increasing from 4.0 and reached to maximum value 7.0. Changing of the buffer solution pH is reason the peak current to drop to. Changing in the pH value shows a low rate for electron transfer in an alkaline and environment response in a solution [35].

3.3 Polyaniline supported PVC/$NiAl_2O_3$/AlF_3/GCE sensor

- Determination of malathion in tomato

A glassy carbon electrode (GCE) coated with a polyaniline-supported PNA nanocomposite was used in standard solutions as an applied sensor for the study of malathion (1.5×10^{-7} to 11×10^{-7} Molar) was modified in 0.2 M KCl and pH 7 [36–38]. A polyaniline-based PNA/GCE electrochemical sensor was used for the detection of malathion in tomatoes harvested under the identical conditions used for the characterization of malathion. The samples containing of the tomato did not contain considerable amounts of malathion and therefore a 4×10^{-7} M malathion solution was added (Table 3).

A reduction experiment was carried out; the experiment was carried out in a quartet. The malathion concentration is 4.94×10^{-7} M in the tomato sample and the rate of the recovery is about 98.4%. The interaction of the polyaniline-based PNA/GCE showed appropriate properties in the linear range and the good detection limit.

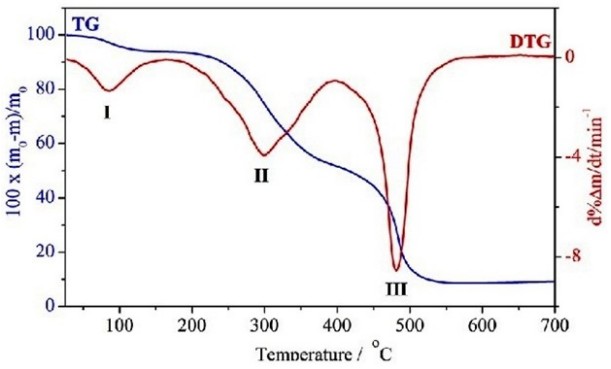

Figure 4. TG-DTG curves for dried samples of $nAlF_3$.

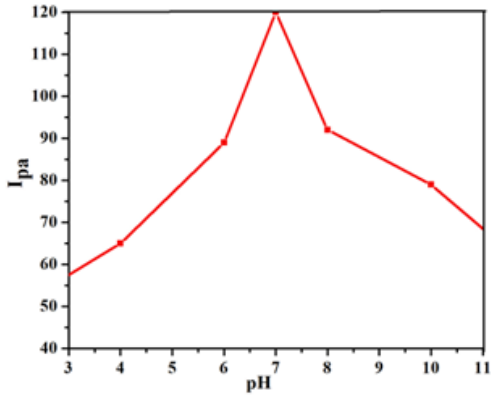

Figure 5. Plot of I_{pa} versus pH obtained using polyaniline supported PVC/NiAl2O3/AlF3/GCE in a malathion solution of 4×10^{-7} M containing 0.2 M KCl. (GCE= Glassy Carbon Electrode).

Table 3. Study of tomato sample by recovery malathion.

No. of Trial	Y(μA)	Malathion added (10^{-7}M)	Found (obtained X in 10^{-7}M)	Recovery (%)
1	5.4	5	4.94	98.1
2	5.3	5	4.97	99.2
3	5.2	5	4.91	98.0
Average	5.3	5	4.94	98.4

4. Conclusion

In the present research, PVC/$NiAl_2O_3$/AlF_3 (PNA) nanocomposite was synthesized by the precipitation method. Polyaniline-based PNA nanocomposites were synthesized by an in situ chemical oxidation method using newly synthesized PNA and $C_6H_5NH_2$ in 0.1 M HCl aqueous solution. All synthetic nanocomposites modified with a GC electrode are controlled by diffusion (reversible redox processes). However, the reversibility of polyaniline-supported PNA nanocomposites is appropriated and this result for the large surface area. Furthermore, the polyaniline-PNA nanocomposite modified GC electrode showed the other pesticides used in the actual malathion sample. Therefore, the PNA/GCE polyaniline advanced performance for analytical and good response (high electron transfer) in optimal condition for the detection of malathion in tomato samples.

Acknowledgment
The financial and encouragement support was provided by the Research Vice Presidency of North Tehran & Tonekabon Branches of Islamic Azad University and Executive Director of Iran-Nanotechnology Organization (Govt. of Iran).

Authors Contributions
Authors had equal role in designing and performing the experiments and preparing the paper.

Availability of Data and Materials
The datasets generated during and/or analyzed during the current study are available from the corresponding author on reasonable request.

Competing interests
The authors have no relevant financial or non-financial interests to disclose.

References

[1] M. E. Turner, T. J. Trentler, and V. L. Colvin. "". *Adv. Mater*, **13**:180–183, 2001.

[2] Aguado, D. P. Serrano, E. Garagorri J. M. Escola, and J. A. Fernandez. "". *Polymer Degradation and Stability*, **69**:11–16, 2000.

[3] P. Gronchi, A. Kaddouri, P. Centola, and R. Del Rosso. "". *J. Sol-Gel Sci. Tech*, **26**:843–846, 2003.

[4] L. Khelifi and A. Ghorbel. "". *J. Sol-Gel Sci Tech*, **19**: 643–646, 2000.

[5] H. Meixner, U. Lampe, J. Gerblinger, and M. Fleische. "". *Fresenius J. Anal. Chem*, **348**:536–541, 1994.

[6] R. A. Bennett and N.D. McCavish. "". *Topics in Catalysis*, **36**:11–19, 2005.

[7] "Chemistry of Advanced Materials: An Overview, Wiely-VCH, Inc, Canada". *Molecular Precursor Routes to Inorganic Solids*, **9**:389–448, 1998.

[8] G. C. Righini and S. Pelli. "". *J. Sol-Gel Sci. Tech*, **8**: 991–997, 1997.

[9] E. Maryani, M. Abdullah, H. Dayamanti, and R. Septawendar. "Effect of ultrasonic irradiation on the characteristic of Y-Al_2O_3 nanorods synthesized from nitrate salt-starch precursors trough a facile precipitation method.". *J. Ceram. Soc. Japan*, **124**:1205–1210, 2016.

[10] A. Amirsalari and S. Farjami. "Effect of pH and calcinations temperature on structural and optical properties of alumina nanoparticles.". *J. Superlatt. Microstruct*, **82**:507–524, 2015.

[11] S. Da-Ros, E. Barbosa-Coutinho, M. Schwaab, V. Calsavara, and N. R. C. Fernandes-Machado. "Modeling the effects of calcination conditions on the physical and chemical properties of transition Alumina catalysts.". *J. Mater. Character*, **80**:50–61, 2013.

[12] A. E. Tayseir Mohammed and M. Saikat. "Some studies on the surface modification of sol-gel derived hydrophilic Silica nanoparticles.". *Int. J. Nano Dimens*, **8**:97–106, 2017.

[13] S. K. Maity, J. Ancheyta, and M. S. Rana. "Support effects on hydroprocessing of maya heavy crude. ". *J. Energy and Fuel*, **19**:343–347, 2005.

[14] V. C. Fernandez, J. Ramrez, A. G. Alejandre, F. Sanchez-Minero, R. Cuevas-Garcıa, and P. Torres-Mancera. "Synthesis, characterization and evaluation of NiMo/SiO_2–Al_2O_3 catalysts prepared by the pH-swing method. ". *J. Catal. Today*, **130**:337–344, 2008.

[15] H. dao Quan, H.Yang, M. Tamura, and A. Sekiya. "". *J. Fluorine Chem*, **125**:1169–1172, 2004.

[16] Sh. Sohrabnezhad, A. Porahmad, M. Razavi, and Murata. "Silver bromide in montmorillonite as visible light-driven photocatalyst and the role of montmorillonite. ". *Applied Physics A*, **122**:522, 2016.

[17] H. dao Quan, M. Tamura, T. Takagi, and A. Sekiya. "". *J. Fluorine Chem*, **99**:167–170, 1999.

[18] C. G. Krespan and D. A. Dixon. "". *J. Fluorine Chem*, **77**:117–126, 1996.

[19] M. A. S. Sadjadi, Babak Sadeghi, M. Meskinfam, K. Zare, and J. Azizian. "". *Physica E: Low-dimensional Systems and Nanostructures*, **40**:3183, 2008.

[20] Babak Sadeghi, M. A. S. Sadjadi, and R. A. R. Vahdati. "". *Superlattices and Microstructures*, **46**:858, 2009.

[21] Babak Sadeghi, M. Jamali, Sh. Kia, A. Amini Nia, and S. Ghafari. "". *Int. J. Nano Dimens*, **1**:119, 2010.

[22] Babak Sadeghi, Farshid S. Garmaroudi, M. Hashemi, H.R. Nezhad, A. Nasrollahi, Sima Ardalan, and Sahar Ardalan. "". *Advanced Powder Technology*, **23**:22, 2012.

[23] Babak Sadeghi and A.Pourahmad. "". *Advanced Powder Technology*, **22**:669, 2012.

[24] Babak Sadeghi, Sh. Ghammamy, Z. Gholipour, M. Ghorchibeigy, and A. Amini Nia. "". *Mic & Nano Letters*, **6**:209, 2011.

[25] Babak Sadeghi. "". *Spectrochimica Acta Part A: Molecular and Biomolecular Spectroscopy*, **118**:787, 2014.

[26] "Babak Sadeghi, Controlled growth and characterization Ag/ZnO nanotetrapods for humidity sensing. ". *Combination Chemistry & High throughput Screening*, **21**:1–6, 2018.

[27] Babak Sadeghi and M. Meskinfam. "". *Spectrochimica Acta Part A: Molecular and Biomolecular Spectroscopy*, **97**:326, 2012.

[28] N. Kaur, M. Singh, A. Moumen, G. Duina, , and E. Comini. "1D titanium dioxide: achievements in chemical sensing.". *Materials*, **13**13:2974, 2020.

[29] A. Pourahmad and F. Azadi. "Synthesis and characterization of a nanocomposite zeolite Y@metal–organic framework as photocatalyst. ". *J. Coordination Chemistry*, **75**:2136–2149, 2022.

[30] A. Umar, T. Almas, A.A. Ibrahim, R. Kumar, M.S. AlAssiri, S. Baskoutas, and M.S. Akhtar. "An efficient chemical sensor based on CeO2 nanoparticles for the detection of acetylacetone chemical. ". *Journal of Electroanalytical Chemistry*, **864**:114089, 2020.

[31] A. Singh, S. Singh, and B.C. Yadav. "Gigantic enhancement in response of heterostructured CeO_2/CdS nanospheres based self-powered CO_2 gas sensor: A comparative study. ". *Sensors and Actuators B: Chemical*, **377**:133085, 2023.

[32] S. Zhao, Y. Shen, F. Hao, C. Kang, B. Cui, D. Wei, and F. Meng. "Pn junctions based on CuO-decorated ZnO nanowires for ethanol sensing application. ". *Applied Surface Science*, **538**:148140, 2021.

[33] G. Hui, M. Zhu, X. Yang, J. Liu, G. Pan, and Z. Wang. "Highly sensitive ethanol gas sensor based on CeO_2/ZnO binary heterojunction composite. ". *Materials Letters*, **278**:128453, 2020.

[34] S. Zhao, Y. Shen, R. Maboudian, C. Carraro, C. Han, W. Liu, and D. Wei. "Facile synthesis of ZnO-SnO_2 hetero-structured nanowires for high-performance NO_2 sensing application. ". *Sensors and Actuators B: Chemical*, **333**:129613, 2021.

[35] T. M. Bekele. "Synthesis and Characterization of CdS/CeO_2 Nanocomposite with Improved Visible-Light Photocatalytic Degradation of Methyl Orange Dye.". , 2021.

[36] A. Valério, F.J. Trindade, R.F. Penacchio, B.C. Ramos, S. Damasceno, M.B. Estradiote, C.B. Rodella, A.S. Ferlauto, S.W. Kycia, and S.L. Morelhao. "Proper usage of Scherrer's and Guinier's formulas in X-ray analysis of size distribution in systems of monocrystalline CeO_2 nanoparticles. ". *arXiv preprint arXiv*, **2203**:00866, 2022.

[37] G. Murugadoss, M. R. Kumar, A. Kathalingam, J.R. Rajabathar, H. Al-Lohedan, and D.M. Al-Dhayan. "Facile synthesis of heterostructure CeO_2/CdS and CdS/CeO_2 nanocomposites for photocatalytic application of methylene blue textile dye. ". *Journal of Ovonic Research*, **17**6, 2021.

[38] Z. Cui, D. Zhang, J. Hu, and C. Fang. "CdS/CeO_2 heterostructures as visible-light photocatalysts for the reduction of nitro to amine organics. ". *Journal of Alloys and Compounds*, **885**:160961, 2021.